Sensitivity analysis of PV produced power in presence of measurement uncertainty

Matteo Intravaia
Department of Information Engineering
Università degli Studi di Firenze
Firenze, Italy
matteo.intravaia@unifi.it

Lorenzo Becchi
Department of Information Engineering
Università degli Studi di Firenze
Firenze, Italy
lorenzo.becchi@unifi.it

Marco Bindi
Department of Information Engineering
Università degli Studi di Firenze
Firenze, Italy
m.bindi@unifi.it

Luigi Costanzo
Department of Engineering
Università della Campania L. Vanvitelli
Aversa (CE), Italy
luigi.costanzo@unicampania.it

Cristian Camilo Garzon Alfonso
Department of Information Engineering
University of Florence
Florence, Italy
garzoncristianc@gmail.com

Vipinkumar Shriram Meshram
Department of Engineering
Università della Campania L. Vanvitelli
Aversa (CE), Italy
vmeshram@unisa.it

Alberto Reatti
Department of Information Engineering
Università degli Studi di Firenze
Firenze, Italy
alberto.reatti@unifi.it

Massimo Vitelli
Department of Engineering
Università della Campania L. Vanvitelli
Aversa (CE), Italy
massimo.vitelli@unicampania.it

2024 IEEE International Workshop on Metrology for Industry 4.0 & IoT (MetroInd4.0 & IoT) | 979-8-3503-8582-3/24/$31.00 ©2024 IEEE | DOI: 10.1109/MetroInd4.0IoT61288.2024.10584219

***Abstract*—Photovoltaics represents one of the key sources of clean energy to help reduce the carbon footprint and fight climate change, enabling the so-called green energy transition. To maximize photovoltaic production in any irradiation and temperature conditions, Maximum Power Point Tracking techniques must be implemented to determine and set the working point at which the photovoltaic panel delivers the maximum power. Such techniques usually exploit real-time measurements of voltage and current on the photovoltaic cell, and possibly of the operating temperature. This paper proposes an assessment of the effects of measurement uncertainty on the maximum power point calculation. We compare the sensitivity to measurement noise of different tracking algorithms, including perturb and observe, incremental conductance and feedforward neural networks. The results show that neural networks become the most attractive solution when measurement uncertainty is introduced in the system.**

Keywords—Maximum Power Point Tracking, Perturb and Observe, Incremental Conductance, Neural Networks

I. INTRODUCTION

Climate change calls for a transition to a more sustainable energy system to support human activities. This process, known as green energy transition [1], poses several challenges, which can be ultimately grouped into two major objectives: first, the increase of the percentage of energy from renewable sources to meet certain goals [2], along with the necessary adaptation of the electricity infrastructure to sustain the passage from centralized to distributed generation; second, the development of new technologies to achieve optimization [3]-[5] and robustness [6]-[9] of production, transmission, distribution, storage and usage of electric energy.

In this context, photovoltaics (PV) represents one of the key sources of clean energy [10]. To maximize the produced energy, it is crucial to ensure that a PV system works at its Maximum Power Point (MPP), which depends on the irradiation and temperature operating conditions. To this aim, MPP Tracking (MPPT) methods must be implemented. The research activity on this topic has produced many approaches to address the MPPT problem. Following the classification proposed in [11], MPPT techniques can be categorized as classic methods, e.g., analytical [12], Perturb and Observe (P&O) [13], Incremental Conductance (IC) [14] and Hill Climbing (HC) [15], intelligent methods, including Artificial Neural Networks (ANNs) [16], [17], optimization-based methods [18], and hybrid methods [19].

Classic methods are capable of achieving high accuracy in the individuation of the MPP, but they perform well only under uniform irradiation conditions. Additionally, as these methods are usually based on iterative algorithms, they tend to be slow and therefore not suited for fine dynamic MPPT. On the other hand, intelligent methods, even though time-consuming in the training phase, can guarantee high tracking speed, allowing for tracking the MPP even in rapidly changing weather conditions. Finally, optimization and hybrid MPPT strategies are best suited under partial shading conditions [20]. In this case, the power-voltage curve of a PV device exhibits multiple local maxima, resulting in the impossibility for algorithms such as P&O, HC, IC and ANNs to identify univocally the global maximum.

All these methods are based on input quantities (typically, current, voltage and temperature) that must be measured on the PV system. Although much scientific effort has been put into developing more accurate and efficient maximum power tracking techniques, only few works have investigated the effects of measurement uncertainty on the tracking capabilities. In [21], the authors study the behavior of an HC algorithm, showing that measurement noise not only slows down the algorithm convergence, but also shifts the settling operating point from the true MPP. Similar considerations are advanced in [22] for IC algorithms. In the work presented in [23], the authors remark the relevance of measurement noise for the MPPT task, proposing a hybrid strategy based on P&O and fuzzy logic.

Starting from these studies, this work specifically focuses on investigating the effects of measurement uncertainty on different MPPT algorithms, attempting to provide a numerical indication of the expected deviation from the actual maximum power for each technique. In particular, the considered MPPT methods are fixed step P&O, adaptive step P&O, IC and ANNs. All the algorithms are tested in a simulated environment on a sample PV panel, modeled with the one-diode equivalent circuit [24], using a realistic irradiance and temperature dataset obtained from PVGIS [25]. The control technique in which these different MPPT approaches are tested involves the direct definition of the solar panel output voltage. As shown in Figure 1, the controller action is commonly used to set the duty cycle of the DC-DC converter applied downstream of the panel (dashed black line output from the gate driver) [26]. In this work the converter is not considered explicitly and the main goal of the algorithms is to set the output voltage reaching the MPP in each operating

979-8-3503-8582-3/23/$31.00 ©2024 IEEE

condition (dashed red line output from the MPPT controller). To the authors' knowledge, this kind of comparative analysis, including also neural networks, has never been conducted before.

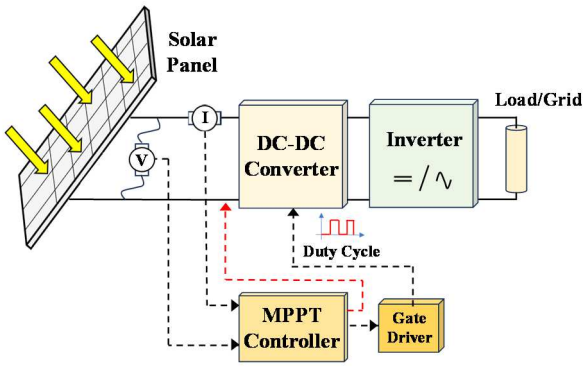

Figure 1 – Block diagram of PV panel connection setup with MPPT controller.

This manuscript is organized as follows: section II provides the necessary theoretical background of the one-diode model, a description of the PVGIS dataset and the details of the implemented MPPT algorithms; section III presents the results of the measurement noise sensitivity analysis, comparing the different MPPT techniques; finally, section IV draws the conclusions.

II. Materials and Methods

A. The one-diode model

The one-diode model, or single-diode model, of a PV panel is represented in Figure 2. Considering such model, the current-voltage (I-V) relationship characterizing the PV panel is given by:

$$i_{pv} = I_{ph} - I_0\left[\exp\left(\frac{v_{PV} + R_s i_{PV}}{n N_s V_T}\right) - 1\right] - \frac{v_{PV} + R_s i_{PV}}{R_{sh}} \qquad (1)$$

where I_{ph} is the photogenerated current, I_0 is the diode dark saturation current, n is the diode ideality factor, N_s is the number of PV cells in series, V_T is the thermal voltage, R_{sh} is the shunt resistance, R_s is the series resistance, v_{PV} and i_{PV} are respectively the voltage and current produced by the PV panel.

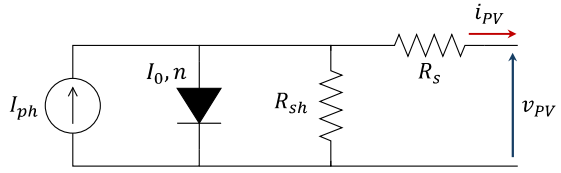

Figure 2 – One-diode model of a PV device.

For a given PV device, the five parameters defining the single-diode model, namely I_{ph}, I_0, R_s, R_{sh} and n, are usually known from datasheet information at Standard Test Conditions (STC), i.e., at the operating temperature $T_{\mathrm{STC}} = 298.15\,K$ with an irradiance $G_{\mathrm{STC}} = 1000\ W/m^2$. From these reference values (see Table 1), indicated in the following with a STC subscript, the values of the parameters in any condition of temperature T and irradiation G can be calculated using the equations:

$$I_{ph}(T,G) = I_{ph,\mathrm{STC}}\frac{G}{G_{\mathrm{STC}}}[1 + \alpha(T - T_{\mathrm{STC}})] \qquad (2)$$

$$I_0(T,G) = I_{0,\mathrm{STC}}\left(\frac{T}{T_{\mathrm{STC}}}\right)^3 \exp\left[\frac{E_{g,\mathrm{STC}}}{kT_{\mathrm{STC}}} - \frac{E_g(T)}{kT}\right] \qquad (3)$$

$$R_s(T,G) = R_{s,\mathrm{STC}} \qquad (4)$$

$$R_{sh}(T,G) = R_{sh,\mathrm{STC}}\frac{G_{\mathrm{STC}}}{G} \qquad (5)$$

$$n(T,G) = n_{\mathrm{STC}} \qquad (6)$$

where α is the PV current temperature coefficient, $E_{g,\mathrm{STC}}$ is the PV cell material energy gap at STC, $E_g(T)$ is the material energy gap at temperature T. Combining equations (2)-(6) with equation (1), it is possible to derive numerically the complete I-V curve of the PV panel, given the working irradiance and temperature. From the I-V characteristic, the maximum power point can be easily individuated. In this study, this procedure is adopted to obtain the actual MPP value in each working condition included in the PVGIS dataset. Such MPP value is used as a reference to evaluate the performance of the tracking algorithms.

B. PV panel module and PVGIS dataset

The study presented in this paper is conducted on a 1SolTech 1-STH-250 solar panel. Table 1 reports the parameters at STC that can be extracted from the manufacturer datasheet. The Nominal Operating Cell Temperature (NOCT) is used to calculate the PV device operating temperature T, given the ambient temperature T_{amb} and the irradiance G, by applying the following formula [27]:

$$T = T_{amb} + (\mathrm{NOCT} - 20)\frac{G}{800} \qquad (7)$$

Table 1 – Parameters at STC of the solar panel model selected for experimentation.

Parameter	Value	Description
N_s	60	Number of cells in series.
$I_{sc,\mathrm{STC}}$	8.66 A	Short-circuit current at STC (usually considered equal to the photogenerated current $I_{ph,\mathrm{STC}}$).
$V_{oc,\mathrm{STC}}$	37.3 V	Open-circuit voltage at STC.
$I_{MP,\mathrm{STC}}$	8.15 A	Current corresponding to the maximum power point at STC.
$V_{MP,\mathrm{STC}}$	30.7 V	Voltage corresponding to the maximum power point at STC.
$I_{0,\mathrm{STC}}$	8.71×10^{-14} A	Dark saturation current
n_{STC}	0.75	Ideality factor
$R_{s,\mathrm{STC}}$	0.35 Ω	Series resistance
$R_{sh,\mathrm{STC}}$	171.64 Ω	Shunt resistance
NOCT	50 °C	Nominal Operating Cell Temperature

A realistic dataset of operating circumstances, including irradiance and ambient temperature, is obtained by using the PVGIS web tool, as mentioned in the Introduction. The dataset under consideration comprises hourly temperature and irradiance data collected over a 30-day period in late summer in the central Italy region (see Figure 3). To acquire a 5-minute temporal granularity, data points with irradiance lower than 50 W/m^2 are deleted and additional data points are added by

interpolation. As such, 3951 operating circumstances are included in the final dataset.

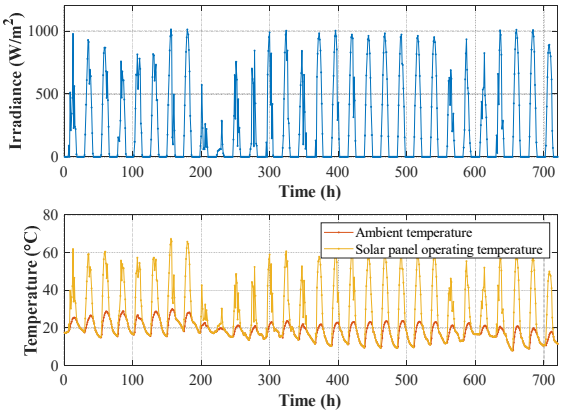

Figure 3 – Hourly irradiance (top) and hourly temperature (bottom) from the selected PVGIS dataset. The solar panel operating temperature is obtained from the ambient temperature and the irradiance applying equation (7).

C. *Maximum Power Point Tracking Techniques*

This section illustrates the working principles of the implemented MPPT techniques.

1) Perturb and Observe

The principle at the basis of P&O techniques is to iteratively impose a variation (perturb) to a quantity (such as voltage, current or converter duty cycle) that influences the PV device behavior, while monitoring the response (observe). The entity of the perturbation can be always the same (fixed step P&O) or change iteration by iteration following some rule (adaptive step P&O), while the direction of the perturbation is established in such a way that the next iteration should move towards the MPP. By repeating this procedure for enough steps, the MPP is eventually reached [13].

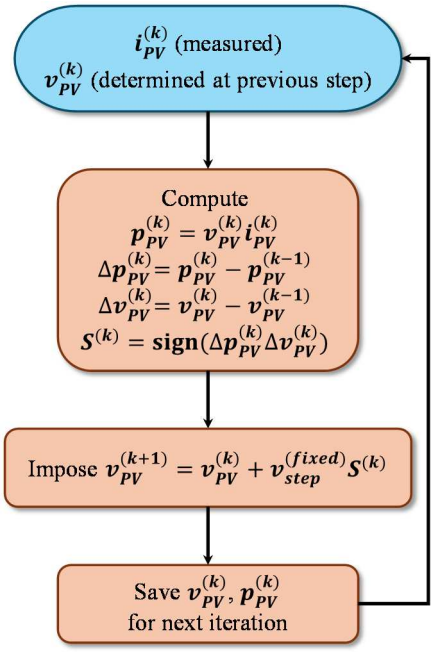

Figure 4 – Flowchart of the implemented fixed step P&O algorithm.

This work features a fixed step and an adaptive step P&O algorithm, both acting on the PV device by imposing the voltage and measuring the current. The workflow of the fixed step P&O is represented in the flowchart in Figure 4. At the beginning of each iteration k, the PV panel current $i_{PV}^{(k)}$ is measured, while its voltage $v_{PV}^{(k)}$ is considered equal to the value imposed at the previous step. Then, the PV power $p_{PV}^{(k)}$, and the quantities $\Delta p_{PV}^{(k)}$ and $\Delta v_{PV}^{(k)}$, can be calculated. The sign of the product $\Delta p_{PV}^{(k)} \Delta v_{PV}^{(k)}$ determines the direction of the next perturbation, which in this case is of fixed amplitude $v_{step}^{(fixed)}$. In this study, $v_{step}^{(fixed)}$ is set equal to 0.1 V.

An adaptive step version of the algorithm is obtained as illustrated in Figure 6. In this case, the magnitude of the perturbation is enlarged of a factor $K_u > 1$ when the working point of the PV panel is far from the MPP and is reduced of a factor $K_d < 1$ as the MPP is approached. More specifically, the implemented algorithm establishes which factor to use at each iteration by comparing the sign of the last two variations, $S^{(k)}$ and $S^{(k-1)}$. If the signs are discordant, it means that the last step surpassed the MPP, therefore the algorithm starts searching backwards with a finer perturbation. In this study, we set heuristically $K_u = 1.3$ and $K_d = 0.5$. Figure 5 visually shows the behavior of the adaptive step algorithm for the first 11 iterations applied on one of the I-V curves obtained from the PVGIS dataset. At the beginning, the algorithm starts searching to the right, increasing the step size at each iteration. When the MPP (red cross) is surpassed (step 4), the algorithm reverses the direction of the next step and halves its amplitude (since K_d is equal to 0.5). The same happens after iterations 6, 8 and 10. The number of iterations is fixed at 200 for both the P&O algorithms.

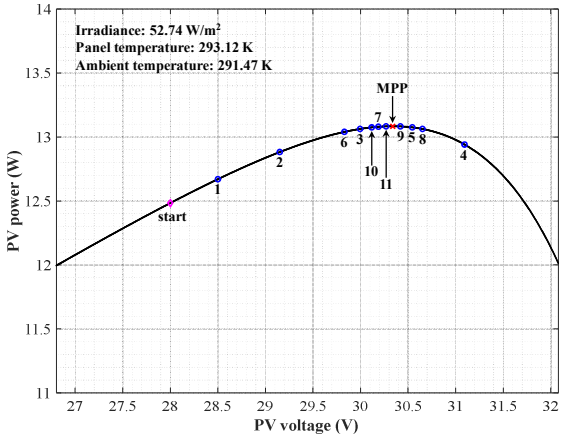

Figure 5 – Behavior of the adaptive step P&O on an example of I-V curve obtained from the PVGIS dataset.

2) Incremental Conductance

The implemented IC method works substantially in the same way as a P&O algorithm, with the difference that the PV voltage at each iteration is updated as follows [28]:

$$v_{PV}^{(k+1)} = v_{PV}^{(k)} + K\left(\frac{\Delta i_{PV}^{(k)}}{\Delta v_{PV}^{(k)}} + \frac{i_{PV}^{(k)}}{v_{PV}^{(k)}}\right) \quad (8)$$

where $\Delta i_{PV}^{(k)} = i_{PV}^{(k)} - i_{PV}^{(k-1)}$ is the variation of the PV panel current from the last two iterations and K is a scaling factor. When the working point approaches the MPP, the quantity in brackets tends to zero. The factor K is set equal to $1\ V^2/A$. As for P&O, the number of iterations of the IC algorithm is 200.

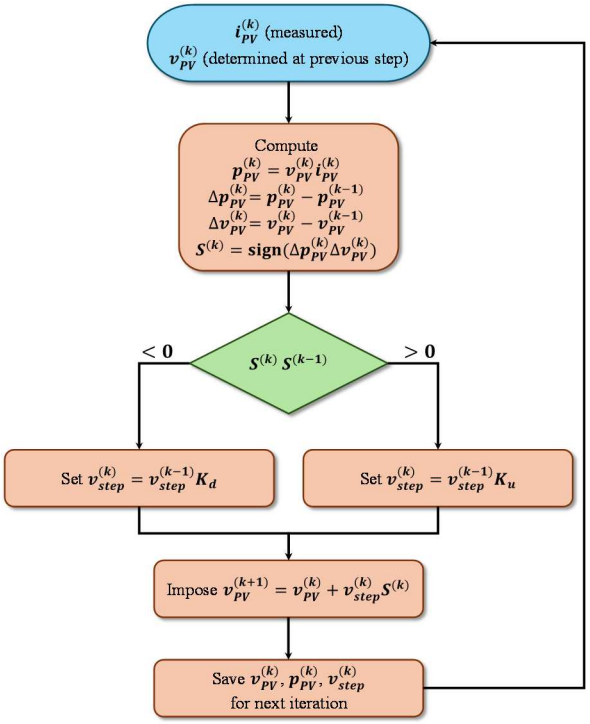

Figure 6 – Flowchart of the implemented adaptive step P&O algorithm.

3) Feedforward Neural Networks

In contrast to P&O and IC, feedforward neural networks (FFNNs) need the operating temperature of the PV device as an input in addition to voltage and current in order to anticipate the converter duty cycle, voltage, or both that correspond to the MPP. The architecture in Figure 7 illustrates how an FFNN with a single hidden layer and 10 neurons is used in this study to predict the MPP voltage V_{MP} from an arbitrary measured point of the I-V curve and the operating temperature, adhering to the methodology previously suggested in [29].

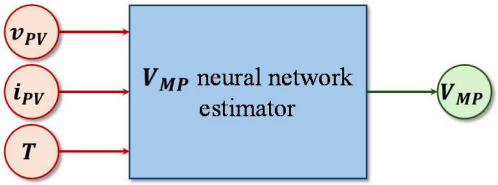

Figure 7 – Block scheme illustrating inputs and outputs of the MPPT algorithm based on neural networks.

The neural network is trained on a specific PV panel model by creating a fictitious dataset of temperature/irradiance operating points. Indicating with n_T and n_G respectively the number of temperature points and the number of irradiance points, in this study we set $n_T = 10$ (equally spaced points from 263.15 K to 353.15 K) and $n_G = 10$ (equally spaced from 200 W/m^2 to 1150 W/m^2), thus creating a grid-like dataset of 100 operating conditions. From the PV panel parameters at STC (see Table 1), using equations (1)-(6), the I-V curve corresponding to each operating condition can be derived. On each curve, it is possible to extract the V_{MP}, which must be the output provided by the neural network for any I-V point of that curve. The resulting dataset is depicted in the plot of Figure 8.

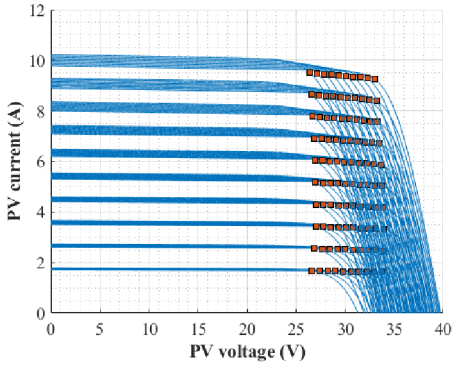

Figure 8 – Representation of the training dataset for the neural network V_{MP} predictor. Each curve corresponds to a temperature/irradiance operating condition. The red squares indicate the MPPs.

III. Results and Discussion

This section presents the results of the application of the MPPT algorithms, illustrated in section II.C, to the dataset extracted from PVGIS. The performance of the algorithms is expressed in terms of Mean Absolute Percentage Error (MAPE). Indicating with N the number of examples in the dataset (in this case, $N = 3951$), with $MPP_{true,j}$ and $\overline{MPP}_j$ respectively the true MPP value and the MPP value found by the tracking algorithm for the j-th example, the MAPE index is computed as:

$$\text{MAPE} = \frac{1}{N}\sum_{j=1}^{N}\left|\frac{MPP_{true,j} - \overline{MPP}_j}{MPP_{true,j}}\right| \qquad (9)$$

In section III.A, the results of the MPPT considering perfect measurements are presented. Section III.B repeats the analysis, but introducing noise on the measurements needed for MPPT.

A. MPPT with perfect measurements

Table 2 reports the MAPE index for the tested MPPT techniques. In addition, the first row of Table 2 indicates a special case where no MPPT is performed and the working voltage of the panel is always set equal to $V_{MP,\text{STC}}$. This represents a baseline reference result that the MPPT algorithms must outperform to be considered viable solutions. The MAPE of the baseline is indicated as MAPE_{bl} In this noise-free test, the adaptive P&O and the IC methods achieve better accuracy, as they are able to precisely adjust the perturbations to arbitrary small values.

Table 2 – MPPT performance in the hypothesis of perfect measurements. The best methods are highlighted in green.

MPPT technique	MAPE
Baseline (no MPPT)	1.720%
P&O fixed step	0.008%
P&O adaptive step	< 0.001%
IC	< 0.001%
FFNN	0.017%

B. MPPT in presence of measurement uncertainty

Table 3 and Table 4 summarize the MPPT results when measurement uncertainty is introduced in the system, respectively for P&O and IC, and for the FFNN. For P&O and

IC, the noise is added to the current measurement at each iteration as a disturbance distributed normally around the nominal value, with a standard deviation equal to a certain percentage of the nominal value (relative uncertainty). For the FFNN, the disturbance is added in the same way on voltage and temperature measurements as well. The relative uncertainties on current, voltage and temperature measurements are indicated respectively as u_I, u_V and u_T. Different levels of uncertainty are considered, ranging from 1% to 20%.

Observing Table 2, Table 3 and Table 4, it is interesting to notice the following aspects:

- When measurement noise is introduced, fixed step P&O is a better option than adaptive P&O and IC. This means that the fixed step size, even if limiting the MPPT accuracy, is somehow beneficial to compensate for the variability of the measurements.
- The method based on neural networks, even if slightly worse than the other techniques in the noise-free scenario, is capable of keeping high tracking accuracy also in heavily disturbed conditions. In particular, the FFNN performance is affected mostly by the uncertainty on temperature measurements, while its sensitivity to errors on voltage and current measurements is extremely limited. This means that neural networks are generally preferable if accurate temperature sensors are available. For instance, a scenario with u_T between 1% and 2% can be a realistic representation of a PV panel equipped with a class B/C PT100 sensor [30].

Table 3 – MPPT results in presence of uncertainty on current measurements for P&O and IC algorithms. An asterisk indicates that the MAPE is greater than $MAPE_{bl}$.

u_I	MAPE		
	P&O fixed step	P&O adaptive step	IC
1%	0.328%	0.472%	*
2%	0.638%	0.936%	*
5%	1.683%	*	*
10%	*	*	*
20%	*	*	*

Table 4 – MPPT results in presence of uncertainty on current, voltage and temperature measurements for the neural network algorithm. An asterisk indicates that the MAPE is greater than $MAPE_{bl}$.

	u_T	0%	1%	2%	5%
u_I, u_V	-	-	-	-	-
0%	-	0.017%	0.097%	0.353%	*
1%	-	0.018%	0.106%	0.362%	*
2%	-	0.029%	0.111%	0.368%	*
5%	-	0.132%	0.208%	0.481%	*
10%	-	0.461%	0.526%	0.764%	*
20%	-	1.022%	1.172%	1.391%	*

IV. Conclusion

This paper presented a comparative analysis of the performance of different MPPT algorithms in presence of measurement noise. The study was conducted in a simulated environment using an irradiance/temperature dataset extracted from PVGIS. Among the tested algorithms (P&O, IC and neural networks), FFNNs proved to be the most robust to voltage and current measurement uncertainty, provided that temperature readings with at maximum 2% uncertainty are available. Conversely, the performance of the other techniques considered in the study considerably worsens when measurement disturbance is introduced.

Moreover, even though neural networks have the drawback of requiring more complex equipment (temperature sensor), on the other hand they hold the important advantage of providing the MPP estimation in a single execution, compared to iterative methods that typically require more time. As such, neural networks appear to be one of the most promising solutions for dynamic MPPT in rapidly changing operating conditions (e.g., for mobile PV systems installed on vehicles [31]).

As regards future developments, we foresee at least two research lines:

- The expansion of the investigation to other MPPT techniques, to provide a thorough overview of the effects of measurement uncertainty and support a more conscious choice of the best solution.
- The implementation of the MPPT algorithms in an MPPT controller (e.g., deployed on a microcontroller) to assess the actual tracking capabilities of each solution in a real working scenario.
- Incorporating voltage and current ripples, particularly at the switching frequency and double the line frequency, is crucial. The amplitudes of the ripple also depend on the PV operating point. These ripples represent additional sources of uncertainty that must be considered for future development.

References

[1] K. Hainsch, K. Löffler, T. Burandt, H. Auer, P. C. del Granado, P. Pisciella and S. Zwickl-Bernhard, "Energy transition scenarios: What policies, societal attitudes, and technology developments will realize the EU Green Deal?," in *Energy*, Volume 239, Part C, 2022, doi: 10.1016/j.energy.2021.122067.

[2] "Directive (EU) 2023/2413 of the European Parliament and of the Council of 18 October 2023 amending Directive (EU) 2018/2001, Regulation (EU) 2018/1999 and Directive 98/70/EC as regards the promotion of energy from renewable sources, and repealing Council Directive (EU) 2015/652," available at: https://eur-lex.europa.eu/legal-content/EN/TXT/?uri=CELEX%3A32023L2413.

[3] F. Corti, M. Intravaia, A. Reatti, F. Grasso, E. Grasso, A. T. Cabrera, "Component design procedure for LCC-S wireless power transfer systems based on genetic algorithms and sensitivity analysis," in *IET Power Electron.*, pp. 1–13, 2024, doi: 10.1049/pel2.12648.

[4] V. S. Meshram, F. Corti, L. Solimene, S. Musumeci, C. S. Ragusa and A. Reatti, "Variable Inductor Control Strategy in LCC-S Compensated Wireless Power Transfer Application," *2023 AEIT International Annual Conference (AEIT)*, Rome, Italy, 2023, pp. 1-6, doi: 10.23919/AEIT60520.2023.10330337.

[5] V. Bertolini, F. Corti, M. Intravaia, A. Reatti, E. Cardelli, "Optimizing power transfer in selective wireless charging systems: A genetic algorithm-based approach," in *Journal of Magnetism and Magnetic Materials*, Volume 587, 2023, doi: 10.1016/j.jmmm.2023.171340.

[6] M. Intravaia *et al.*, "Prognostic Analysis of Switching Devices in DC-DC Converters," *2023 IEEE International Conference on Metrology for eXtended Reality, Artificial Intelligence and Neural Engineering (MetroXRAINE)*, Milano, Italy, 2023, pp. 224-229, doi: 10.1109/MetroXRAINE58569.2023.10405672.

[7] M. Bindi, M. C. Piccirilli, A. Luchetta, F. Grasso, S. Manetti, "Testability Evaluation in Time-Variant Circuits: A New Graphical Method," in *Electronics* 2022, 11, 1589, doi: 10.3390/electronics11101589.

[8] C. A. Iturrino Garcia, M. Bindi, F. Corti, A. Luchetta, F. Grasso, L. Paolucci, M. C. Piccirilli, I. Aizenberg, "Power Quality Analysis Based on Machine Learning Methods for Low-Voltage Electrical Distribution Lines," in *Energies* 2023, 16, 3627, doi: 10.3390/en16093627.

[9] M. Intravaia *et al*., "Predictive Maintenance of Actuated Quarter-Turn Valves Using Artificial Intelligence," *2023 IEEE International Conference on Metrology for eXtended Reality, Artificial Intelligence and Neural Engineering (MetroXRAINE)*, Milano, Italy, 2023, pp. 149-154, doi: 10.1109/MetroXRAINE58569.2023.10405793.

[10] T. Addabbo *et al*., "Solar energy harvesting for LoRaWAN-based pervasive environmental monitoring," in *Acta IMEKO*, Volume 10, Issue 2, pp. 111-118, 2021, doi: 10.21014/acta_imeko.v10i2.1046.

[11] R. B. Bollipo, S. Mikkili and P. K. Bonthagorla, "Hybrid, optimal, intelligent and classical PV MPPT techniques: A review," in *CSEE Journal of Power and Energy Systems*, vol. 7, no. 1, pp. 9-33, Jan. 2021, doi: 10.17775/CSEEJPES.2019.02720.

[12] A. Laudani *et al*., "An analytical approach for maximum power point calculation for photovoltaic system," *2017 European Conference on Circuit Theory and Design (ECCTD)*, Catania, Italy, 2017, pp. 1-4, doi: 10.1109/ECCTD.2017.8093270.

[13] R. Kahani, M. Jamil and M. T. Iqbal, "An Improved Perturb and Observed Maximum Power Point Tracking Algorithm for Photovoltaic Power Systems," in *Journal of Modern Power Systems and Clean Energy*, vol. 11, no. 4, pp. 1165-1175, July 2023, doi: 10.35833/MPCE.2022.000245.

[14] N. Kumar, I. Hussain, B. Singh and B. K. Panigrahi, "Self-Adaptive Incremental Conductance Algorithm for Swift and Ripple-Free Maximum Power Harvesting From PV Array," in *IEEE Transactions on Industrial Informatics*, vol. 14, no. 5, pp. 2031-2041, May 2018, doi: 10.1109/TII.2017.2765083.

[15] Y. Liu *et al*., "An MPPT Approach Using Improved Hill Climbing and Double Closed Loop Control," *2019 IEEE 46th Photovoltaic Specialists Conference (PVSC)*, Chicago, IL, USA, 2019, pp. 2935-2941, doi: 10.1109/PVSC40753.2019.8980863.

[16] A. Laudani, F. R. Fulginei, A. Salvini, G. M. Lozito and F. Mancilla-David, "Implementation of a neural MPPT algorithm on a low-cost 8-bit microcontroller," *2014 International Symposium on Power Electronics, Electrical Drives, Automation and Motion*, Ischia, Italy, 2014, pp. 977-981, doi: 10.1109/SPEEDAM.2014.6872101.

[17] M. Bindi *et al*., "Comparison Between PI and Neural Network Controller for Dual Active Bridge Converter," *2021 IEEE 15th International Conference on Compatibility, Power Electronics and Power Engineering (CPE-POWERENG)*, Florence, Italy, 2021, pp. 1-6, doi: 10.1109/CPE-POWERENG50821.2021.9501168.

[18] S. Mohanty, B. Subudhi and P. K. Ray, "A New MPPT Design Using Grey Wolf Optimization Technique for Photovoltaic System Under Partial Shading Conditions," in *IEEE Transactions on Sustainable Energy*, vol. 7, no. 1, pp. 181-188, Jan. 2016, doi: 10.1109/TSTE.2015.2482120.

[19] S. Mohanty, B. Subudhi and P. K. Ray, "A Grey Wolf-Assisted Perturb & Observe MPPT Algorithm for a PV System," in *IEEE Transactions on Energy Conversion*, vol. 32, no. 1, pp. 340-347, March 2017, doi: 10.1109/TEC.2016.2633722.

[20] A. Mohapatra, B. Nayak, P. Das and K. B. Mohanty, "A review on MPPT techniques of PV system under partial shading condition," in *Renewable and Sustainable Energy Reviews*, Volume 80, 2017, doi: 10.1016/j.rser.2017.05.083.

[21] H. Al-Atrash, I. Batarseh and K. Rustom, "Effect of Measurement Noise and Bias on Hill-Climbing MPPT Algorithms," in *IEEE Transactions on Aerospace and Electronic Systems*, vol. 46, no. 2, pp. 745-760, April 2010, doi: 10.1109/TAES.2010.5461654.

[22] M. A. Elgendy, B. Zahawi and D. J. Atkinson, "Assessment of the Incremental Conductance Maximum Power Point Tracking Algorithm," in *IEEE Transactions on Sustainable Energy*, vol. 4, no. 1, pp. 108-117, Jan. 2013, doi: 10.1109/TSTE.2012.2202698.

[23] M.A.A.M. Zainuri, M.A.M. Radzi, A. Che Soh and N.A. Rahim, "Development of adaptive perturb and observe-fuzzy control maximum power point tracking for photovoltaic boost dc–dc converter," in *IET Renewable Power Generation*, 8, 183-194, 2014, doi: 10.1049/iet-rpg.2012.0362.

[24] A. Laudani, G. M. Lozito, F. R. Fulginei, "Irradiance Sensing through PV Devices: A Sensitivity Analysis," in *Sensors*, 2021, 21, 4264, doi: 10.3390/s21134264.

[25] "Photovoltaic Geographical Information System (PVGIS)," https://joint-research-centre.ec.europa.eu/photovoltaic-geographical-information-system-pvgis_en.

[26] V. S. Meshram and A. Reatti, "Performance Analysis of Zeta Converter for Photovoltaic Powered Micromobility Charging Station," *2023 AEIT International Annual Conference (AEIT)*, Rome, Italy, 2023, pp. 1-5, doi: 10.23919/AEIT60520.2023.10330345.

[27] V. Sun, A. Asanakham, T. Deethayat and T. Kiatsiriroat, "Evaluation of nominal operating cell temperature (NOCT) of glazed photovoltaic thermal module," in *Case Studies in Thermal Engineering*, Volume 28, 2021, doi: 10.1016/j.csite.2021.101361.

[28] A. Safari and S. Mekhilef, "Simulation and Hardware Implementation of Incremental Conductance MPPT With Direct Control Method Using Cuk Converter," in *IEEE Transactions on Industrial Electronics*, vol. 58, no. 4, pp. 1154-1161, April 2011, doi: 10.1109/TIE.2010.2048834.

[29] M. Bertoluzzo *et al*., "Neural Networks for Maximum Power Point Tracking Application to Silicon and CIGS Photovoltaic Modules," *2018 IEEE 4th International Forum on Research and Technology for Society and Industry (RTSI)*, Palermo, Italy, 2018, pp. 1-6, doi: 10.1109/RTSI.2018.8548445.

[30] International Electrotechnical Commission, "IEC 60751:2022. Industrial platinum resistance thermometers and platinum temperature sensors."

[31] G. Talluri, M. Bindi, A. Luchetta, F. Grasso, L. Luchetti and L. Paolucci, "Analysis of Power Losses due to Magnetic Shielding for Electric Vehicle Wireless Charging," *2021 IEEE 15th International Conference on Compatibility, Power Electronics and Power Engineering (CPE-POWERENG)*, Florence, Italy, 2021, pp. 1-6, doi: 10.1109/CPE-POWERENG50821.2021.9501223.